Low-Lying Excited States of 7-Aminocoumarin Derivatives: A Theoretical Study

TETSUYA SAKATA,[1] YUKIO KAWASHIMA,[1,2] HARUYUKI NAKANO[1]

[1]*Department of Chemistry, Graduate School of Sciences, Kyushu University, Fukuoka 812-8581, Japan*

[2]*Organization for the Promotion of Advanced Research, Kyushu University, Fukuoka 812-8581, Japan*

Received 22 October 2008; accepted 24 November 2008
Published online 6 March 2009 in Wiley InterScience (www.interscience.wiley.com).
DOI 10.1002/qua.22019

ABSTRACT: Excited states of three 7-aminocoumarin derivatives, coumarin 120 (7-amino-4-methylcoumarin), pyrrolyl coumarin 7-(1*H*-pyrrol-1-yl)-4-methyl-2*H*-1-benzopyran-2-one, and carbazole-coumarin hybrid 10*H*-4-methyl-2*H*-2-oxopyrano[5,6-*b*]carbazole, have been studied using B3LYP time-dependent density functional theory (TDDFT). The solvent effect has been taken into account using the polarizable continuum model. The spectra calculated using TDDFT agree well with the experimental absorption spectra. The electronic structures and the solvent effect for the low-lying singlet excited states have been investigated. The HOMO of the pyrrolyl coumarin is localized on the pyrrolyl ring, while the HOMO in the other 7-aminocoumarins is delocalized over the entire molecule. This leads to the weak fluorescence of the pyrrolyl coumarins found in experiments. The HOMO and next HOMO in carbazole-coumarin hybrids have similar orbital energy values, which is not the case in the other 7-aminocoumarin derivatives. This leads to the additional peaks found in the 30,000–40,000 cm^{-1} region of the observed absorption spectra, which are specific for carbazole-coumarin hybrids. Int J Quantum Chem 109: 1940–1949, 2009

Key words: excited states; 7-aminocoumarin; B3LYP; TDDFT; solvent effect

Correspondence to: Y. Kawashima; e-mail: snow@ccl.scc.kyushu-u.ac.jp

This article is dedicated to Professor Kimihiko Hirao at the occasion of his retirement from University of Tokyo.

Contract grant sponsors: Special Coordination Funds for Promoting Science and Technology [SCF, Program for Improvement of Research Environment for Young Researchers], Japan; CREST, Japan Science and Technology Agency (JST).

Introduction

The excited states of 7-aminocoumarin derivatives have been studied extensively both experimentally [1–13] and theoretically [13–21] because of their interesting photophysical properties. These molecules are highly fluorescent and thus widely used as laser dyes in the blue-green region, solar energy concentrators, and nonlinear optical chromophores. The large state-dependent variation of the dipole moment causes a large Stokes shift for these molecules, which is sensitive to the polarity of solvents. Thus, 7-aminocoumarin dyes have also been used in studying solvatochromic properties in solvents.

In spite of the large amount of research and wide applications of 7-aminocoumarins, further investigation of the excited states is essential. For the past two decades, the nonradiative deactivation mechanism of 7-aminocoumarins has been debated. The first model describes the nonradiative deactivation process as the 7-aminocoumarin forming the so-called twisted intramolecular charge transfer state from the S_1 singlet excited state [3]. The second is the so-called open-closed umbrella-like motion mechanism [4]. This mechanism ascribes the internal conversion process to a structural change of the amino group from a planar N^+-aromatic configuration (with sp^2 hybridization for the nitrogen atom) to a pyramidal N-aromatic configuration (with sp^3 hybridization for the nitrogen atom). For coumarin 120 (C120) [10] and coumarin 151 (C151) [9], it is known that the nonradiative deactivation process differs in polar and nonpolar solvents.

Various quantum mechanical methods have been employed to study the excited states of 7-aminocoumarins. Semiempirical excited state calculations of 7-aminocoumarins in the gas phase have been reported by McCarthy and Blanchard [14]. Ando [15] combined ab initio electronic structure calculations and molecular dynamics simulation to study the solvation dynamics of C120 in methanol. A Car-Parrinello molecular dynamics (CPMD) simulation was carried out to study microsolvated C151 [16, 17], coumarin 35 (C35) [17], and coumarin 153 (C153) [17] utilizing the QM/MM CPMD method [22]. Cave et al. [18] have performed time-dependent density functional theory (TDDFT), CASSCF, and multistate CASPT2 calculations for coumarin C120 and C151. Kurashige et al. [19] have applied TDDFT, configuration interaction singles, and resolution-of-the-identity CC2 to coumarin 343

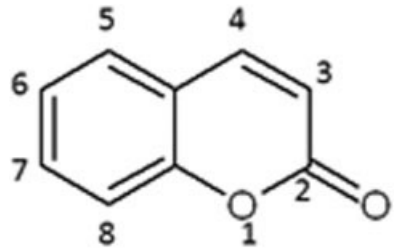

FIGURE 1. Molecular structure of coumarin with the numbering of skeletal atoms.

and its derivatives. The most widely used method for studying the excited states of aminocoumarin derivatives is the TDDFT method. C153 has been studied by Mühlpfordt et al. [13] in the gas phase, and by Improta et al. [21] in cyclohexane solution. Nguyen et al. [20] applied various density functionals and basis sets to C120, C102, coumarin 1, coumarin 152, C35, coumarin 522, C153, coumarin 307, and C151 and assessed their performance.

Recently, Kitamura et al. [1] reported a systematic study of the synthesis, absorption, and fluorescence of 17 7-aminocoumarin derivatives. They discussed the effect of alkylation of the amino group at the 7-position, trifluoromethylation of the methyl group at the 4-position, and the number of ring structures on the absorption and fluorescence spectra. The numbering of the skeletal atoms of coumarin is shown in Figure 1. In their observations, the absorption spectra of the carbazole-coumarin hybrids (compounds **12**–**15** in Ref. [1]) had two peaks in the 30,000−40,000 cm^{-1} region, an observation that was not made for the other 7-aminocoumarin derivatives. In the fluorescence spectra, they found that pyrrolyl coumarins (compounds **7**–**9** in Ref. [1]) exhibit weak fluorescence, while most of the other 7-aminocoumarins showed strong fluorescence. To our knowledge, the character of the excited states of these derivatives has not been studied in detail theoretically so far.

The aim of this article is to elucidate the character of the low-lying excited states of 7-aminocoumarin derivatives. We have chosen three 7-aminocoumarins with different character in the low-lying excited states from Ref. [1] to explore: coumarin 120 (7-amino-4-methylcoumarin, compound **1** in Ref. [1]), 7-(1*H*-pyrrol-1-yl)-4-methyl-2*H*-1-benzopyran-2-one (compound **7** in Ref. [1]) for pyrrolyl coumarins, and 10*H*-4-methyl-2*H*-2-oxopyrano[5,6-*b*]carbazole (compound **12** in Ref. [1]) from the carbazole-coumarin hybrids. The three de-

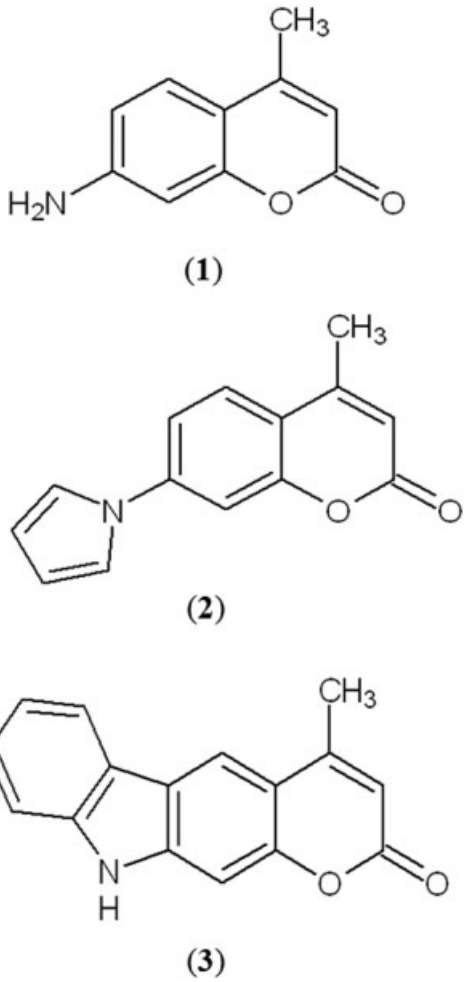

FIGURE 2. Chemical structures of the 7-aminocoumarins: (**1**) Coumarin 120, (**2**) 7-(1*H*-pyrrol-1-yl)-4-methyl-2*H*-1-benzopyran-2-one, (**3**) 10*H*-4-methyl-2*H*-2-oxopyrano[5,6-*b*] carbazole.

rivatives chosen are illustrated in Figure 2. TDDFT was used to explore the excited states of these 7-aminocoumarin derivatives in the gas phase and in ethanol. This article is organized as follows. The computational details are described in the next section. The results of the calculations are shown and discussed in the third section. The article is concluded in the final section.

Computational Details

The calculations were carried out for the ground and low-lying singlet excited states of coumarin 120 (referred to as **1** hereafter), 7-(1*H*-pyrrol-1-yl)-4-methyl-2*H*-1-benzopyran-2-one (referred to as **2** hereafter), and 10*H*-4-methyl-2*H*-2-oxopyrano[5,6-*b*]-carbazole (referred to as **3** hereafter). The ground state geometries of the 7-aminocoumarins studied were optimized at the DFT level, so the excitation energies obtained from our calculation are vertical in nature. The excitation energy calculations were carried out applying TDDFT [23–28]. We used Becke's three-parameter B3LYP hybrid functional [29–31] for all of our DFT and TDDFT calculations. To consider the solvent effect, we applied the polarizable continuum model (PCM) [32–34]. The dielectric constant $\varepsilon = 24.55$ was used in our PCM calculation to estimate the solvent effect of ethanol. Dunning's cc-pVDZ [35] was used for our calculation. The geometry optimizations and the TDDFT calculations were all performed with the GAUSSIAN03 suite of programs [36].

Results and Discussion

THE GROUND STATE STRUCTURE OF 7-AMINOCOUMARIN DERIVATIVES

The ground state structure of the coumarin moiety of the 7-aminocoumarin derivatives in the gas phase and ethanol are listed in Table I. The molecular structure designation is illustrated in Figure 3. The bonds are designated by letters (a–k) and the bond angles are designated by numbers (1–15).

Bonds a–f belong to the aromatic ring. Bonds c and d have the largest deviation because the differences in the compounds are mainly at the 7-position in Figure 1. Compared with the bonds in the aromatic ring, the bonds g–j, which show large bond alternations, do not show much deviation among the aminocoumarin derivatives.

The bonds a–f in ethanol are elongated in all of these compounds compared with those in the gas phase. However, the solvent effect on the aromatic ring in **2** is small compared with other compounds. The dipole moment of the amino group is reduced by the formation of the pyrrolyl ring. This leads to a reduction in the solvent effect on the aromatic ring of the coumarin moiety in polar solvents. The bond alternations in bonds g–k are reduced in ethanol.

The bond angles have a smaller deviation among the 7-aminocoumarin derivatives and the solvent effect is small as well. The sum of the bond angles around the nitrogen atom in **1** is 345.5° in the gas phase. The amino group in **1** is pyramidal and not

TABLE I

Optimized geometry of the 7-aminocoumarin derivatives.

	1		2		3	
	Gas	Ethanol	Gas	Ethanol	Gas	Ethanol
Bond length (Å)						
a	1.409	1.416	1.408	1.411	1.406	1.411
b	1.383	1.383	1.385	1.388	1.390	1.392
c	1.414	1.423	1.408	1.411	1.427	1.433
d	1.401	1.409	1.396	1.399	1.392	1.397
e	1.391	1.391	1.394	1.395	1.392	1.393
f	1.412	1.414	1.410	1.410	1.421	1.423
g	1.448	1.445	1.453	1.454	1.453	1.452
h	1.360	1.368	1.358	1.363	1.358	1.365
i	1.452	1.444	1.455	1.449	1.453	1.447
j	1.400	1.391	1.399	1.391	1.396	1.388
k	1.363	1.371	1.362	1.368	1.365	1.372
Bond angle (°)						
1	116.9	116.7	117.2	117.1	118.6	118.5
2	121.8	121.7	121.6	121.6	120.3	120.1
3	120.4	120.7	120.0	120.1	119.2	119.5
4	118.9	118.5	119.7	119.7	122.1	121.9
5	119.9	119.8	119.6	119.4	117.2	117.1
6	122.1	122.6	121.9	122.2	122.6	123.0
7	116.4	117.8	125.8	125.8	125.0	125.1
8	116.3	117.6	125.8	125.6	109.8	109.6
9	112.8	114.3	108.4	108.6	125.1	125.2
Sum (7–9)	345.5	349.7	360.0	360.0	360.0	360.0
10	118.2	118.4	118.1	118.3	117.7	117.8
11	118.8	118.8	118.6	118.5	119.0	119.0
12	123.1	122.6	123.3	122.9	123.2	122.8
13	116.0	116.9	116.0	116.8	116.0	116.8
14	122.3	122.2	122.2	122.0	122.6	122.4
15	121.6	121.2	121.8	121.7	121.5	121.2

planar as in the other compounds. In spite of the planar structure around the nitrogen, **2** has a twisted structure. The pyrrolyl group plane and the coumarin moiety plane have a dihedral angle of 28.1° and 30.8° in the gas phase and in ethanol, respectively.

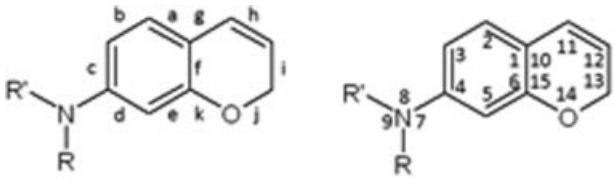

FIGURE 3. Designation of bonds and bond angles of the 7-aminocoumarins.

THE EXCITED STATES OF 7-AMINOCOUMARIN DERIVATIVES

The calculated excitation energy and the observed absorption spectra in Ref. [1] are shown in Figure 4. Figures 4(a)–(c) correspond to the calculated results of compounds **1**, **2**, and **3**, respectively. Overall, the spectral shapes of the calculated results obtained utilizing TDDFT and PCM agree very well with the experimental absorption spectra obtained in ethanol. To study in detail the difference in the absorption spectra among the three compounds, we chose the first seven states for **1** and 10 states for **2** and **3** that contribute to the absorption spectra. The occupied orbitals of the 7-aminocoumarin derivatives are designated by 1, 2, 3, . . . , from the highest one down, and the unoccupied orbitals by 1′, 2′, 3′, . . . , from the lowest one up.

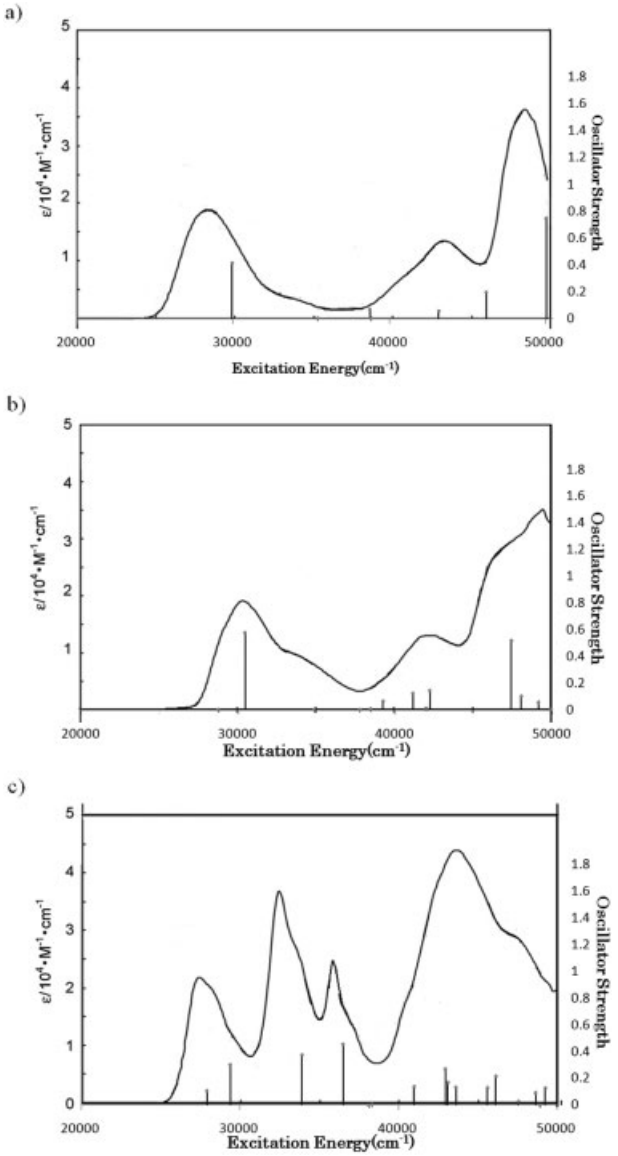

FIGURE 4. The absorption spectra of the 7-aminocoumarins: (a) **1**, (b) **2**, and (c) **3**. The lines show the calculated excitation energies and the curves are the absorption spectra observed in Ref. [1].

The Excited States of 1

The molecular orbitals of **1** are illustrated in Figure 5(a). The main configurations of the obtained excited states are shown in Table II. The calculated excitation energies and the oscillator strength are listed in Table III. The first excited state of **1** results from the 1 (HOMO) $\rightarrow$ 1′ (LUMO) transition, where orbital 1 is a π orbital and 1′ is a π^* orbital. This state has a large oscillator strength, thus we have assigned this state to the first peak located near 28,000 cm^{-1} in the experimental spectrum in Figure 4(a). The excitation energy in ethanol is 3.71 eV, which is 0.20 eV higher than the experimental value. Consideration of the solvent effect leads to a large red shift of 0.28 eV for this $\pi \rightarrow \pi^*$ excited state.

The next two excited states are both described by 1 $\rightarrow$ 2′ (next LUMO) and 2 (next HOMO) $\rightarrow$ 1′ transitions, where 2 is a π orbital and 2′ is a π^* orbital. The oscillator strength of the second state is smaller than that of the third state. In studies of the excited states of polyacenes [37–39], the electric dipole transition moment vectors for the one-electron 2 $\rightarrow$ 1′ and 1 $\rightarrow$ 2′ transitions are similar in magnitude and parallel in their orientation. These two transitions give rise to the pseudoparity-forbidden $^1B_{3u}^-$ state with lower excitation energy and a dipole-allowed $^1B_{3u}^+$ state with higher excitation energy. The two transition moments cancel each other in the lower state and add up in the higher state. The excited states of compound **1** show a similar tendency to the polyacene case. These $\pi \rightarrow \pi^*$ excited states show red shifts because of ethanol, as in the first excited state.

The fourth excited state has a different character compared with the other excited states. The excitation energy shows a strong blue shift, because this excited state is described as the 4 $\rightarrow$ 1′ transition, where 4 is the orbital of the lone pair electrons of the oxygen atom of C═O. The stabilization of the lone pair because of the solvent increases the excitation energy.

The main configurations of the fifth and sixth excited states are 3 $\rightarrow$ 1′ and 1 $\rightarrow$ 3′ transitions, where 3 is a π orbital and 3′ is a π^* orbital. As in the second and third states, the latter has a larger oscillator strength. These two states are shifted to the red in ethanol like the other $\pi \rightarrow \pi^*$ excited states. We have assigned this sixth state to the second peak of the observed absorption spectrum found in the range 43,000–44,000 cm^{-1}. The seventh state has the largest oscillator strength of 0.7454 in ethanol. We have assigned this to the third peak near 39,000 cm^{-1}. This state is described as the 2 $\rightarrow$ 2′ transition. We have obtained the excitation energy of 6.21 eV in ethanol.

The Excited States of 2

The molecular orbitals of **2** are illustrated in Figure 5(b). Tables IV and V list the main configurations of the calculated excited states and the calculated excitation energies with the oscillator strengths, respectively. Among the molecular orbit-

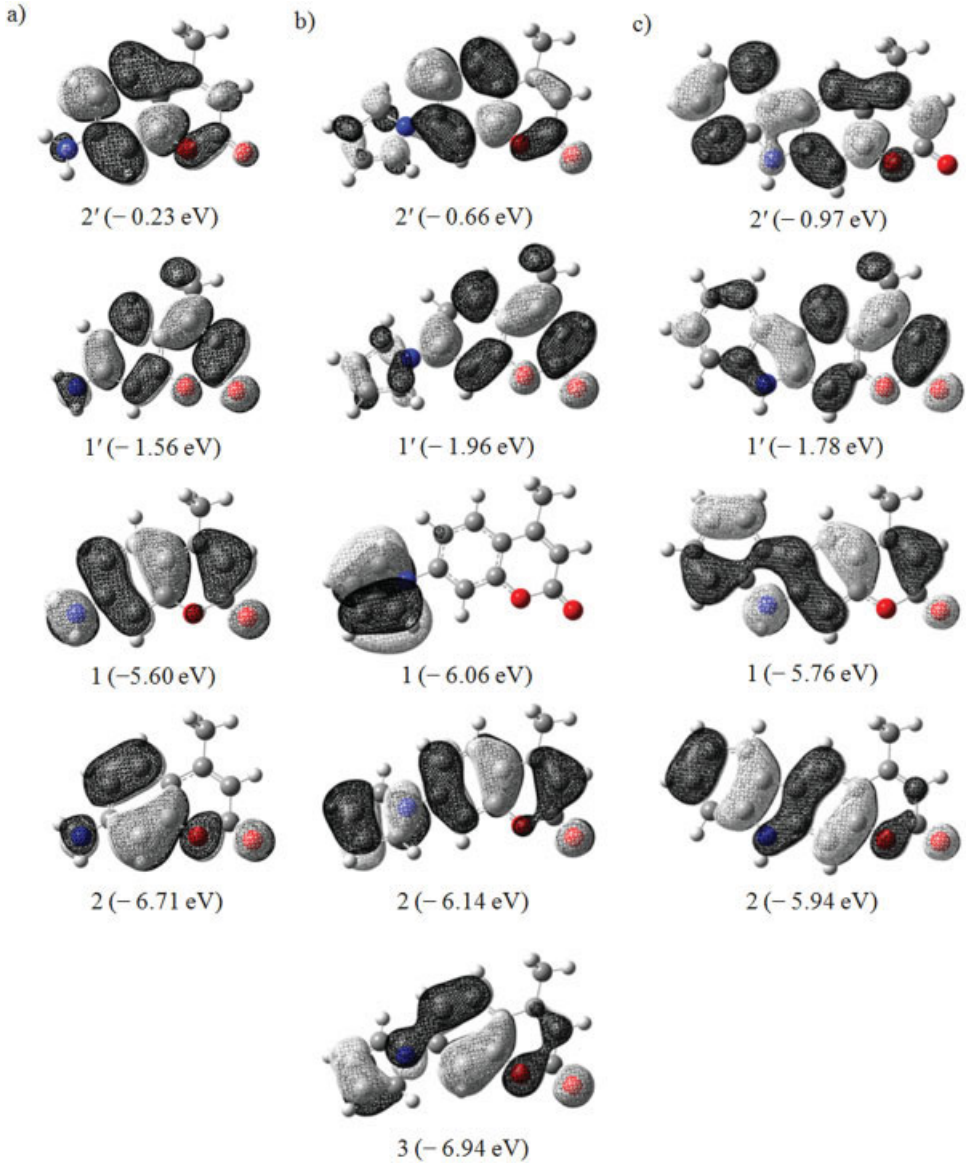

FIGURE 5. Molecular orbitals of the 7-aminocoumarins: (a) **1**, (b) **2**, and (c) **3**. The orbital energies are given in parentheses. [Color figure can be viewed in the online issue, which is available at www.interscience.wiley.com.]

als found in Table IV, molecular orbital 5 is the lone pair of the oxygen atom of C═O, while 4, 3, 2, and 1 are π orbitals and 1′, 2′, and 3′ are π^* orbitals. The $\pi \rightarrow \pi^*$ excited states of **2** show a smaller red shift compared with **1**. This is due to the small solvent effect on the aromatic ring of the coumarin moiety.

The HOMO, or 1, is localized on the pyrrolyl ring. The character of 1 has changed dramatically compared with **1**, which has a delocalized π character. This results in a large decrease in the oscillator strength of the first $\pi \rightarrow \pi^*$ excited state of **2**, described by the $1 \rightarrow 1'$ transition. This explains the low fluorescence found in **2** [1]. The change in 1 also has an influence on the other excited states.

The next HOMO, or 2, has a similar character to the HOMO in **1**, and molecular orbital 3 of **2** has a similar character to the next HOMO in **1**. The transition $2 \rightarrow 1'$, which corresponds to $1 \rightarrow 1'$ in **1**, gives rise to an excited state with a strong oscillator strength of 0.5764 in ethanol. This second excited state of **2** is assigned to the first peak obtained in the observed spectrum shown in Figure 4(b), located near 30,000 cm^{-1}. The excitation energy calculated using TDDFT was 3.77 eV in ethanol, which agrees

TABLE II

Main configurations in the excited states of 1 obtained using TDDFT.

State	Singlet transitions	Coefficients
1^1A	$1 \rightarrow 1'$	0.641
2^1A	$2 \rightarrow 1'$	0.591
	$1 \rightarrow 2'$	–0.353
3^1A	$1 \rightarrow 2'$	0.531
	$2 \rightarrow 1'$	0.326
4^1A	$4 \rightarrow 1'$	0.661
5^1A	$1 \rightarrow 3'$	0.521
	$3 \rightarrow 1'$	–0.430
6^1A	$3 \rightarrow 1'$	0.460
	$1 \rightarrow 3'$	0.351
7^1A	$2 \rightarrow 2'$	0.557

with the experimental data. The third state with a $\pi \rightarrow \pi^*$ character comes from transitions $3 \rightarrow 1'$ and $2 \rightarrow 2'$, which cancel each other and lead to a small oscillator strength. This state corresponds to the second excited state of **1**, described by transitions $2 \rightarrow 1'$ and $1 \rightarrow 2'$.

The fourth excited state has a large blue shift of 0.24 eV. The nature of this state is $n \rightarrow \pi^*$. The fifth, sixth, and seventh excited states are $\pi \rightarrow \pi^*$ excited states. The fifth state is described by the transition $1 \rightarrow 2'$, the sixth state by $2 \rightarrow 2'$, $4 \rightarrow 1'$, and $3 \rightarrow 1'$, and the seventh state by $4 \rightarrow 1'$, $2 \rightarrow 2'$, and $3 \rightarrow 2'$. The excitation energies for the fifth, sixth, and seventh excited states are 4.77, 4.86, and 5.10 eV, respectively. One-electron transitions $1 \rightarrow 3'$ and $2 \rightarrow 3'$ give rise to the eighth and ninth excited states with $\pi \rightarrow \pi^*$ character. The latter have smaller oscillator strength than the former. The excitation energies of the eighth and ninth excited states are predicted to be 5.10 and 5.23 eV, respectively. We have assigned the seventh and ninth excited states to the second peak of the observed absorption spectrum near 42,000 cm^{-1}. The tenth excited state is a $\pi \rightarrow \pi^*$ excited state with large oscillator strength. The excitation energy was found to be 5.87 eV in ethanol and arises from the transitions $3 \rightarrow 2'$ and $4 \rightarrow 2'$. The tenth state was assigned to the peak above 46,000 cm^{-1}. This state corresponds to the

TABLE III

Calculated singlet excitation energies (eV) of 1.

State	TDDFT (Gas)	TDDFT (Ethanol)	Experiment
1^1A	4.03 (0.3234)	3.71 (0.4138)	3.51[a]
2^1A	4.48 (0.0012)	4.39 (0.0041)	
3^1A	5.02 (0.0393)	4.80 (0.0667)	
4^1A	4.54 (0.0001)	4.82 (0.0045)	
5^1A	5.51 (0.0130)	5.35 (0.0555)	
6^1A	5.95 (0.1398)	5.73 (0.1960)	
7^1A	6.31 (0.5517)	6.21 (0.7454)	

The oscillator strengths are given in parentheses.
[a] Ref. [1].

TABLE IV

Main configurations in the excited states of 2 obtained using TDDFT.

State	Singlet transitions	Coefficients
1^1A	$1 \rightarrow 1'$	0.696
2^1A	$2 \rightarrow 1'$	0.657
3^1A	$3 \rightarrow 1'$	0.626
	$2 \rightarrow 2'$	–0.229
4^1A	$5 \rightarrow 1'$	0.673
5^1A	$1 \rightarrow 2'$	0.689
6^1A	$2 \rightarrow 2'$	0.487
	$4 \rightarrow 1'$	–0.389
	$3 \rightarrow 1'$	–0.243
7^1A	$4 \rightarrow 1'$	0.482
	$2 \rightarrow 2'$	0.307
	$3 \rightarrow 2'$	0.221
8^1A	$1 \rightarrow 3'$	0.598
	$2 \rightarrow 3'$	–0.313
9^1A	$2 \rightarrow 3'$	0.547
	$1 \rightarrow 3'$	0.294
10^1A	$3 \rightarrow 2'$	0.579
	$4 \rightarrow 2'$	0.203

TABLE V

Calculated singlet excitation energies (eV) of 2.

State	TDDFT (Gas)	TDDFT (Ethanol)	Experiment
1^1A	3.57 (0.0012)	3.56 (0.0019)	
2^1A	3.89 (0.4488)	3.77 (0.5764)	3.77[a]
3^1A	4.36 (0.0012)	4.32 (0.0016)	
4^1A	4.44 (0.0019)	4.68 (0.0015)	
5^1A	4.75 (0.0036)	4.77 (0.0067)	
6^1A	4.89 (0.0493)	4.86 (0.0647)	
7^1A	5.20 (0.0546)	5.10 (0.1248)	
8^1A	5.26 (0.0024)	5.20 (0.0100)	
9^1A	5.35 (0.1476)	5.23 (0.1447)	
10^1A	5.89 (0.1857)	5.87 (0.5190)	

The oscillator strengths are given in parentheses.
[a] Ref. [1].

TABLE VI
Main configurations in the excited states of 3 obtained using TDDFT.

State	Singlet transitions	Coefficients
1^1A	$1 \rightarrow 1'$	0.626
	$2 \rightarrow 1'$	–0.253
2^1A	$2 \rightarrow 1'$	0.600
	$1 \rightarrow 2'$	–0.217
	$1 \rightarrow 1'$	0.217
3^1A	$1 \rightarrow 2'$	0.622
4^1A	$2 \rightarrow 2'$	0.609
5^1A	$5 \rightarrow 1'$	0.677
6^1A	$3 \rightarrow 1'$	0.630
7^1A	$4 \rightarrow 1'$	0.510
	$1 \rightarrow 3'$	–0.417
8^1A	$2 \rightarrow 3'$	0.437
	$3 \rightarrow 2'$	–0.335
	$1 \rightarrow 3'$	0.290
9^1A	$4 \rightarrow 1'$	0.420
	$1 \rightarrow 3'$	0.385
	$2 \rightarrow 3'$	–0.279
10^1A	$3 \rightarrow 2'$	0.501
	$2 \rightarrow 3'$	0.313
	$2 \rightarrow 4'$	–0.203

seventh excited state of **1** dominated by the $2 \rightarrow 2'$ transition.

The Excited States of 3

The molecular orbitals of **3** are illustrated in Figure 5(c). The main configurations of the calculated excited states and the calculated excitation energies with the oscillator strengths are listed in Tables VI and VII, respectively. Among the molecular orbitals found in Table VI, V is the lone pair of the oxygen atom of C═O, while 4, 3, 2, and 1 are π orbitals and 1′, 2′, 3′, and 4′ are π^* orbitals. The $\pi \rightarrow \pi^*$ excited states of **3** show strong red shifts, as in **1**.

We found that the first four calculated $\pi \rightarrow \pi^*$ excited states have a high oscillator strength. The first peak of the observed absorption spectrum near 27,000 cm^{-1} shown in Figure 4(c) is assigned to the first two excited states calculated using TDDFT. The first excited state is described by transitions $1 \rightarrow 1'$ and $2 \rightarrow 1'$, while the second is described by $2 \rightarrow 1'$, $1 \rightarrow 2'$, and $1 \rightarrow 1'$. The obtained excitation energies for the first and second states are 3.46 and 3.65 eV, respectively. The excitation energy calculated using TDDFT agrees well with the experimental value of 3.40 eV. The third excited state is dominated by the $1 \rightarrow 2'$ transition. The excitation energy in ethanol is 4.20 eV. This state is assigned to the second peak in the experimental absorption spectrum near 32,500 cm^{-1}. Transition $2 \rightarrow 2'$ gives rise to the fourth excited state. The excitation energy calculated using TDDFT was 4.53 eV in ethanol. We have assigned this state to the third peak of the experimental absorption spectrum near 36,000 cm^{-1}.

In the excited states of **3**, the π orbitals 1 and 2 have similar orbital energies, and both orbitals have delocalized π structure along the long π-conjugated systems that have the same number of nodes in the π orbital. The elongation of the π-conjugated network leads to the mixing of transitions $1 \rightarrow 1'$ and $2 \rightarrow 1'$ found in the first and second excited states of **3**, which was not seen in the excited states of **1** or **2**. The two transitions do not cancel each other, thus the first two excited states in **3** both have a high oscillator strength. Transition $1 \rightarrow 2'$ does not pair with $2 \rightarrow 1'$, which has a similar magnitude of electron transition dipole moment vector with a parallel orientation. The cancellation found in the excited states of **1** and **2** does not occur because the orbital energy difference is large. This leads to the large transition dipole moment to the third excited state. The $2 \rightarrow 2'$ transition with a large transition dipole moment is lower in energy than for **1** and **2** ($3 \rightarrow 2'$ in the case of **2**) because orbital 2 has a similar orbital energy to HOMO. This explains the origin of the two peaks in the range 30,000–40,000 cm^{-1}, which were not seen in the other 7-aminocoumarin derivatives.

TABLE VII
Calculated singlet excitation energies (eV) of 3.

State	TDDFT (Gas)	TDDFT (Ethanol)	Experiment
1^1A	3.71 (0.0060)	3.46 (0.1043)	3.40[a]
2^1A	3.79 (0.2584)	3.65 (0.3005)	
3^1A	4.37 (0.2066)	4.20 (0.3721)	
4^1A	4.63 (0.5154)	4.53 (0.4520)	
5^1A	4.48 (0.0000)	4.73 (0.0000)	
6^1A	4.94 (0.0049)	4.75 (0.0054)	
7^1A	5.20 (0.0407)	5.08 (0.1359)	
8^1A	5.37 (0.1444)	5.32 (0.2682)	
9^1A	5.48 (0.0188)	5.34 (0.1668)	
10^1A	5.57 (0.3336)	5.41 (0.1297)	

The oscillator strengths are given in parentheses.
[a] Ref. [1].

The fifth excited state is an $n \rightarrow \pi^*$ excited state with a strong blue shift. The next $\pi \rightarrow \pi^*$ state is located just above the fifth excited state. This sixth excited state has a main configuration of $3 \rightarrow 1'$, with a small oscillator strength like the fifth state. We have assigned the next four $\pi \rightarrow \pi^*$ excited states to the peak observed in the range 40,000–50,000 cm^{-1} in the experimental absorption spectrum. The excitation energies of the seventh, eighth, ninth, and tenth excited states are 5.08, 5.32, 5.34, and 5.41 eV, respectively. The seventh state consists of transitions $4 \rightarrow 1'$ and $1 \rightarrow 3'$, the eighth state consists of $3 \rightarrow 2'$, $2 \rightarrow 3'$, and $1 \rightarrow 3'$, the ninth state consists of $4 \rightarrow 1'$, $1 \rightarrow 3'$, and $2 \rightarrow 3'$, and the tenth state consists of $3 \rightarrow 2'$, $2 \rightarrow 3'$, and $2 \rightarrow 4'$.

Conclusions

We have studied the low-lying excited states of three 7-aminocoumarin derivatives employing TD-DFT with PCM. The predicted excitation energies and the spectral shape are in good agreement with the observed results.

We found that the solvent effect of ethanol leads to a red shift in the excitation energies for the $\pi \rightarrow \pi^*$ excited states, and a blue shift for the $n \rightarrow \pi^*$ excited states. The pyrrolyl coumarin **2** shows a small red shift compared with the other coumarin derivatives. This is due to the small solvent effect on the ground state structures of the aromatic ring in the coumarin moiety.

We have elucidated the electronic structures of the 7-aminocoumarins studied in this article. Among the 7-aminocoumarin derivatives, pyrrolyl coumarin **2** has a HOMO localized on the pyrrolyl ring while the HOMO in the other 7-aminocoumarins is delocalized over the entire molecule. This leads to the reduction of the oscillator strength in the first excited state. This is consistent with the experimental results, which report that the pyrrolyl coumarins exhibit low fluorescence. The experimental absorption spectra of carbazole-coumarin hybrids show two peaks in the range 30,000–40,000 cm^{-1}, which were not seen in the other 7-aminocoumarin derivatives. Our calculated results reproduce these peaks. The HOMO and next HOMO of carbazole-coumarin hybrid **3** has similar orbital energy values, because of the long π conjugation, which is specific to carbazole-coumarin hybrids.

References

1. Kitamura, N.; Fukagawa, T.; Kohtani, S.; Kitoh, S.; Kunimoto, K.; Nakagaki, R. J Photochem Photobiol A Chem 2007, 188, 378.
2. Nakagaki, R.; Kitamura, N.; Aoyama, I.; Ohtsubo, H. J Photochem Photobiol A Chem 1994, 90, 113.
3. Jones, G, II; Jackson, W. R.; Choi, C.-Y.; Bergmark, W. R. J Phys Chem 1985, 89, 294.
4. Arbeloa, T. L.; Arbeloa, F. L.; Tapia, M. J.; Arbeloa I. L. J Phys Chem 1993, 97, 4704.
5. Arbeloa, T. L.; Arbeloa, F. L.; Arbeloa, I. L. J Lumin 1996, 68, 149.
6. Gustavsson, T.; Cassara, T. L.; Gulbinas, V.; Gurzadyan, G.; Mialocq, J.-C.; Pommeret, S.; Sorgius, M.; van der Meulen, P. J Phys Chem A 1998, 102, 4229.
7. Chen, Y.; Palmer, P. M.; Topp, M. R. Int J Mass Spectrom 2002, 220, 231.
8. Sharma, V. K.; Saharo, P. D.; Sharma, N.; Rastogi, R. C.; Ghoshal, S. K.; Mohan, D. Spectrochim Acta Part A 2003, 59, 1161.
9. Nad, S.; Pal, H. J Phys Chem A 2001, 105, 1097.
10. Pal, H.; Nad, S.; Kumbhakar, M. J Chem Phys 2003, 119, 442.
11. Das, K.; Jain, B.; Patel, H. S. J Phys Chem A 2006, 110, 1698.
12. Moog, R. S.; Kim, D. D.; Oberle, J. J.; Ostrowski, S. G. J Phys Chem A 2004, 108, 9294.
13. Mühlpfordt, A.; Schanz, R.; Ernsting, N. P.; Farztdinov, V.; Grimme, S. Phys Chem Chem Phys 1999, 1, 3209.
14. McCarthy, P. K.; Blanchard, G. J. J Phys Chem 1993, 97, 12205.
15. Ando, K. J Chem Phys 1997, 107, 4585.
16. Neugebauer, J.; Jacob, C. R.; Wesolowski, T. A.; Baerends, E. J. J Phys Chem A 2005, 109, 7805.
17. Sulpizi, M.; Röhrig, U. F.; Hutter, J.; Rothlisberger, U. Int J Quantum Chem 2004, 101, 671.
18. Cave, R. J.; Burke, K.; Castner E. W., Jr. J Phys Chem A 2002, 106, 9294.
19. Kurashige, Y.; Nakajima, T.; Kurashige, S.; Hirao, K.; Nishikitani, Y. J Phys Chem A 2007, 111, 5544.
20. Nguyen, K. A.; Day, P. N.; Pachter, R. J Chem Phys 2007, 126, 094303.
21. Improta, R.; Barone, V.; Santoro, F. Angew Chem 2007, 119, 409.
22. Sulpizi, M.; Carloni, P.; Hutter, J.; Rothlisberger, U. Phys Chem Chem Phys 2003, 5, 4798.
23. Runge, E.; Gross, E. K. U. Phys Rev Lett 1984, 52, 997.
24. Casida, M. E. Recent Advances in Density Functional Methods; Chong, D. P., Ed.; World Scientific: Singapore, 1995; Vol. 1, p 155.
25. Bauernschmitt, R.; Ahlrichs, R. Chem Phys Lett 1996, 256, 454.
26. Stratmann, R. E.; Scuseria, G. E.; Frisch, M. J. J Chem Phys 1998, 109, 8218.
27. Furche, F.; Ahlrichs, R. J Chem Phys 2002, 117, 7433.
28. Furche, F.; Ahlrichs, R. J Chem Phys 2004, 121, 12772.
29. Becke, A. D. J Chem Phys 1993, 98, 5648.

30. Becke, A. D. Phys Rev A 1988, 38, 3098.
31. Lee, C.; Yang, W.; Parr, R. G. Phys Rev B 1988, 37, 785.
32. Tomasi, J.; Mennucci, B.; Cammi, R. Chem Rev 2005, 105, 2999.
33. Cossi, M.; Barone, V. J Chem Phys 2001, 115, 4708.
34. Improta, R.; Barone, V.; Scalmani, G.; Frisch, M. J Chem Phys 2006, 125, 54103.
35. Dunning, T. H. J Chem Phys 1989, 90, 1007.
36. Frisch, M. J.; Trucks, G. W.; Schlegel, H. B.; Scuseria, G. E.; Robb, M. A.; Cheeseman, J. R.; Montgomery, J. A., Jr.; Vreven, T.; Kudin, K. N.; Burant, J. C.; Millam, J. M.; Iyengar, S. S.; Tomasi, J. J.; Barone, V.; Mennucci, B.; Cossi, M.; Scalmani, G.; Rega, N.; Petersson, G. A.; Nakatsuji, H.; Hada, M.; Ehara, M.; Toyota, K.; Fukuda, R.; Hasegawa, J.; Ishida, M.; Nakajima, T.; Honda, Y.; Kitao, O.; Nakai, H.; Klene, M.; Li, X.; Knox, J. E.; Hratchian, H. P.; Cross, J. B.; Adamo, C.; Jaramillo, J.; Gomperts, R.; Stratmann, R. E.; Yazyev, O.; Austin, A. J.; Cammi, R.; Pomelli, C.; Ochterski, J. W.; Ayala, P. Y.; Morokuma, K.; Voth, A.; Salvador, P.; Dannenberg, J. J.; Zakrzewski, V. G.; Dapprich, S.; Daniels, A. D.; Strain, M. C.; Farkas, O.; Malick, D. K.; Rabuck, A. D.; Raghavachari, K.; Foresman, J. B.; Ortiz, J. V.; Cui, Q.; Baboul, A. G.; Clifford, S.; Cioslowski, J.; Stefanov, B. B.; Liu, G.; Liashenko, A.; Piskorz, P.; Komaromi, I.; Martin, R. L.; Fox, D. J.; Keith, T.; Al-Laham, M. A.; Peng, C. Y.; Nanayakkara, A.; Challacombe, M.; Gill, P. M. W.; Johnson, B.; Chen, W.; Wong, M. W.; Gonzalez, C.; Pople, J. A. Gaussian 03, Revision D. 02; Gaussian, Inc.: Wallingford, CT, 2004.
37. Hashimoto, T.; Nakano, H.; Hirao, K. J Chem Phys 1996, 104, 6244.
38. Hashimoto, T.; Nakano, H.; Hirao, K. J Mol Struct (Theochem) (Huzinaga Special Issue) 1998, 451, 25.
39. Kawashima, Y.; Hashimoto, T.; Nakano, H.; Hirao, K. Theor Chem Acc (Fukui Special Issue) 1999, 102, 49.